A RESEARCH OF NUMERICAL SIMULATION ON ARGON MAGNETIC FLUID

Zhongping Zhao, Ruiping Xiong*, Junhong Yang, Xing Hu

School of Mechanical Engineering, Sichuan University, Chengdu, 610065, China

*Corresponding author: xiongruiping214@outlook.com

An argon magnetic fluid is a collection of free charged particles moving in random directions especially that is a weakly ionized argon discharge and on the average, electrically neutral. Two-dimensional numerical steady-state model of an argon magnetic fluid generator is presented to investigate the thermodynamic behaviors and the distribution of current density. Computational fluid dynamics codes, OpenFOAM and Fluent, are utilized in a modified form to model the argon magnetic flow inside the generator. Modeling a thermal magnetic fluid requires a combination of mutually related fluid dynamics and electromagnetic phenomena. With the appropriate thermophysical model, a pressure-based, steady-state, incompressible magnetic fluid solver based on OpenFOAM was originally developed. Meanwhile, Fluent was expanded upon secondary development functions of User-Defined Scalar and User-Defined Function to develop magnetic fluid solution and make reference comparison. The results demonstrated that the numerical simulations obtained with the OpenFOAM solver were in good agreement with those from Fluent. The highest temperature and velocity were both observed near the cathode region, with the main body temperature exceeding 6000 K. The anode region exerted a compressive effect on the temperature field and accelerated the magnetohydrodynamic flow. The current density was primarily distributed in a columnar pattern, concentrated in the cathode region and exponentially decreasing along the axis towards the anode region, with a significant radial gradient.

Key words*: Magnetohydrodynamics; Numerical simulation; OpenFOAM's solver; Fluent secondary development*

1. Introduction

Due to the harsh working conditions in turbojet engines, gas turbines, and similar fields, there are extremely high demands on device components for high temperature resistance, wear resistance, and corrosion resistance. Ordinary metal materials often typically fall short of meeting these stringent requirements, while materials with high melting points and hardness present challenges for plastic processing. As a result, surface ceramic coating technology has emerged as an ideal solution, offering the best of both worlds choice [1-4]. Metal powder spheroidization is essential for effective surface coating, and magnetic fluid jets provide an ideal heat source for this process. They offer advantages such as high temperatures, high energy flow density, low operational and maintenance costs, and minimal environmental requirements [5, 6]. Consequently, the application and research of magnetic

fluid have become a major focus in the field of ceramic coating preparation on metal surfaces in recent years.

An argon magnetic fluid is a collection of free charged particles moving in random directions that is, on the average, electrically neutral. This study deals with weakly ionized argon discharges, which have the following features: (a) they are driven electrically; (b) charged particle collisions with neutral gas molecules are important; (c) ionization of neutrals sustains the magnetic fluid in the steady state; and (d) the electrons are not in thermal equilibrium with the ions. A simple discharge can be succinctly understood as a voltage source drives current through a low-pressure argon gas between two parallel conducting plates or electrodes. The gas "breaks down" to form a magnetic fluid, usually weakly ionized. The magnetic fluid medium is complicated in that the charged particles are both excited and affected by external electric and magnetic fields and contribute to them. The velocity distribution of the flow is significantly modified by the arising of Lorentz forces, meanwhile, a substantial amount of heat is released during this process [7, 8].

Due to the high temperature and complex physical fields involved, existing detection methods struggle to effectively evaluate this process [9]. Therefore, relying on modern finite volume method, numerical calculation provides a valid way to understand this complex physical behavior inside the generator [10, 11]. The modeling of magnetic fluid is an extremely challenging task because the magnetic flow is highly nonlinear and presents strong property gradients. Despite the complexity of the subject, over the past few decades, A wealth of literature concerning numerical studies of the characteristics of magnetic fluid have been published. Hsu K.C. [12] obtained the physical field distribution law of two-dimensional (2D) free burning normal pressure argon arc through sub-regional modeling and using appropriate boundary conditions. Chen X. [13] made a detailed derivation of the basic equations and electromagnetic field equations in the magnetic fluid continuum region, and scientifically simplified the two-dimensional rotationally symmetric magnetic fluid mathematical model. Literature [14] established a two-dimensional axially symmetric magnetohydrodynamic model and obtained the results of arc temperature, velocity and current density characteristics. Sun JH. [15] developed a 2D two-temperature chemical non-equilibrium model by adopted two different sets of chemical kinetic process to investigate the plasma characteristics inside a DC arc plasma torch of argon. Sass-Tisovskaya [16] developed a solver through the open source software OpenFOAM (OF) and introduced the calculation formula of magnetic fluid physical properties. However, there is a certain deviation in the results observed in the area near the cathode. Godinaud [17] developed a compressible magnetic fluid solver by incorporating the properties of the magnetic fluid into the state equation through interpolation based on temperature and pressure. However, this approach encounters challenges due to the large and complex nature of the calculations. It is clearly that at the initial stage, a 2D model was employed in the research to predict the heat transfer and flow patterns inside the generator, but are limited to systems where there is axial symmetry. The assumption of axial symmetry in 2D modeling is legit when arc attachment shows a diffusive behavior, which is only valid for conditions of high current and low gas flow. With the rapid development of computer technology, the calculation of heat transfer and fluid flow for a 3D thermal magnetic fluid with axisymmetric geometries became feasible, which also introduces a series of challenges such as overwhelming computational requirements and calculations fail to converge [18, 19]. While 2D models have limitations in capturing detailed features, they can accurately describe the thermodynamic behaviors

within a magnetic flow domain under specific conditions. Moreover, they offer significant advantages in computational efficiency and convergence over 3D models.

In this research, a pressure-based, steady-state, laminar, incompressible argon magnetic fluid solver based on OF is originally developed to solve the 2D rotationally symmetric magnetohydrodynamics model. The solver obtains the temperature, velocity, and current density distributions, especially, which is mutually corroborated with the same case from a customized Fluent simulation. This comparison validates the mathematical theory of magnetic fluids and provides a foundational numerical simulation method for the design and optimization of magnetic fluid industrial applications.

2. Mathematical Modeling

2.1. Assumptions of the simulation

This study investigates the macroscopic characteristics of magnetic fluids. Therefore, reasonable simplifications and assumptions about the argon magnetic fluid can not only avoid many minor issues that do not significantly affect the research but also simplify calculations and enable more efficient results. The details are as follows:

I. The magnetic fluid is steady-state, rotationally symmetric, optically thin, and laminar.
II. The magnetic fluid is assumed to be in a local thermodynamic equilibrium state (LTE).
III. The effects of gravity and viscous dissipation are ignored.
IV. The magnetic fluid is considered as incompressible, and all its thermophysical properties are functions of temperature only.

Based on the above assumptions, the magnetohydrodynamic model will be greatly simplified. In this model, the electric field intensity has no tangential component, while the magnetic induction intensity generated by the current consists solely of a tangential component.

2.2. Governing equations

The magnetohydrodynamic model primarily consists of two components: the fluid-governing Navier-Stokes (N-S) equations and the electromagnetic field-coupling Maxwell equations. These two major systems of equations are integrated by incorporating source terms into the N-S Equations.

I. Mass conservation equation:

$$\nabla \cdot (\rho \mathbf{U}) = 0 \tag{1}$$

II. Momentum conservation equation:

$$\nabla \cdot (\rho \mathbf{U}\mathbf{U}) = -\nabla p + \nabla \cdot [\mu(\nabla \mathbf{U} + (\nabla \mathbf{U})^{\top}) - \frac{2}{3}\mu(\nabla \cdot \mathbf{U})] + \mathbf{J} \times \mathbf{B} \tag{2}$$

III. Enthalpy conservation equations:

$$\nabla \cdot (\rho \mathbf{U} h) = \nabla \cdot (\frac{\kappa}{c_p} \nabla h) + \mathbf{J} \cdot \mathbf{E} + \frac{5}{2} k_B \frac{\mathbf{J}}{e} \cdot \frac{\nabla h}{c_p} - U_r \tag{3}$$

IV. Poisson equation for the electric potential:

$$\nabla \cdot (\sigma \nabla \phi) = 0 \tag{4}$$

V. Ampere's law:

$$\nabla^2 \mathbf{A} = -\mu_0 \mathbf{J} \quad (5)$$

VI. Ohm's law:

$$\mathbf{J} = \sigma \mathbf{E} \quad (6)$$

VII. Electric field intensity equation:

$$\mathbf{E} = -\nabla \phi \quad (7)$$

VIII. Magnetic induction intensity equation:

$$\mathbf{B} = \nabla \times \mathbf{A} \quad (8)$$

where a self-induced magnetic field **B** is generated around current flow through the magnetic fluid, which is obtained by the magnetic vector potential **A** from Eq. (8). The magnetic vector potential **A** is determined from the Ampere's law. Current density **J** is obtained from the current continuity equation $\nabla \cdot \mathbf{J} = 0$, along with the generalized Ohm's law $\mathbf{J} = \sigma(-\nabla\phi + \mathbf{U} \times \mathbf{B})$. However, this study assumes that the induction-less approximation is valid, considering the magnetic flow with a low fluid velocity and magnetic permeability. Therefore, the $\mathbf{U} \times \mathbf{B}$ term can be neglected, which also explains why the Poisson equation for the electric potential is presented in the form of Eq. (4) rather than its general form $\nabla \cdot (\sigma \nabla \phi) = \nabla \cdot (\sigma \mathbf{U} \times \mathbf{B})$.

The N-S Equations are modified to include the additional source terms such as Lorentz force term $\mathbf{J} \times \mathbf{B}$, Joule heating term $\mathbf{J} \cdot \mathbf{E}$, electron enthalpy flux $5/2 \cdot k_B \cdot (\mathbf{J}/e) \cdot (\nabla h / c_p)$ and magnetic fluid thermal radiation loss $-U_r$ in the momentum and energy equations along with electromagnetic relations.

2.3. Properties interpolation method

Generally speaking, the thermophysical properties of substances such as density, molecular viscosity, specific heat capacity, and thermal conductivity are usually assumed to be constants for simplicity. However, since the maximum temperature of argon magnetic fluid can reach up to 30000 K, multiple ionization-recombination reactions occur as the temperature increases. The continuous variation in particle composition prevents the properties from being treated as constant. Therefore, it is necessary to scientifically characterize the thermophysical properties of argon magnetic fluid.

According to the 4*th* item of the assumption, the study uses the properties-temperature table [20] as the basis to complete the properties calculation through simple linear interpolation [21]. Taking the example of the interpolation of thermal conductivity from a thermal conductivity-temperature table, first an index is computed by

$$i = \left\lfloor \left| \left(\frac{T - T_0}{\mathrm{d}T} \right) \right| \right\rfloor \quad (9)$$

where T is the current temperature, T_0 is the first set of the temperature value in the table, and $\mathrm{d}T$ is the distance between the table values. Secondly, the table temperature is computed by

$$T_{tab} = T_0 + i \cdot \mathrm{d}T \quad (10)$$

finally, the interpolation is achieved by

$$\kappa = \kappa_{tab}(i) + (\kappa_{tab}(i+1) - \kappa_{tab}(i)) \cdot \left(\frac{T - T_{tab}}{\mathrm{d}T} \right) \quad (11)$$

where $\kappa_{tab}(i)$ is the ith value in the thermal conductivity table.

It is worth noting that this interpolation method only makes sense if the current temperature T falls within the temperature range specified in the table. Therefore, the current temperature must be normalized before performing attribute interpolation calculation.

3. Computational Modeling

3.1. Design of the domain

The case configured for the validation of the OF solver and Fluent originally comes from the research of Perambadur [19]. The geometry is modified and shown in Fig. 1, whose size information is show in Tab. 1.

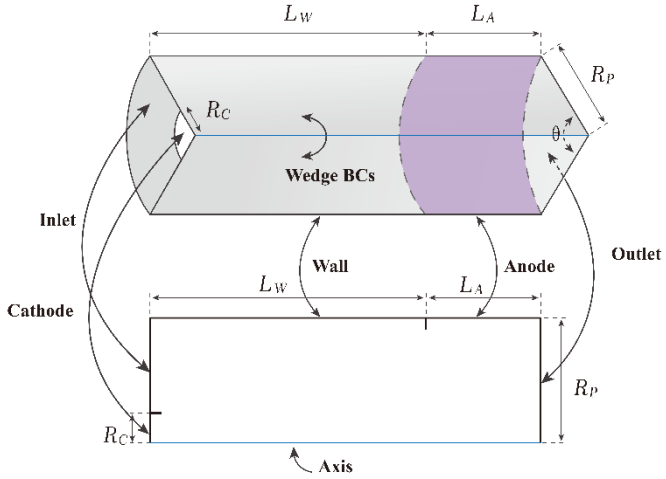

Figure 1. Magnetic fluid calculation model

Table 1. Details of the calculation model

Part	Symbol	Length (mm)
Cathode	R_C	1
Wall	L_W	60
Anode	L_A	40
Outlet	R_P	10

As shown in the three-dimensional model, in the solver of the OF software, a wedge-shaped calculation domain with a wedge angle θ less than 5° and a wedge boundary type is adopted to simplify calculations for the two-dimensional rotationally symmetric model. Similarly, in the two-dimensional model, Fluent software can directly use a planar grid with the Axisymmetric Swirl option to achieve the same goal.

The magnetic fluid enters the computational domain through the Inlet, triggering the ionization-recombination reaction between the Cathode and the Anode. This reaction produces a high-temperature and high-speed flame that ejects from the Outlet.

3.2. Boundary conditions

Appropriate boundary conditions are crucial for obtaining optimal results in numerical simulations. Boundary conditions details of the present work are given in Tab.2.

The computational domain mainly has 6 parts of boundaries (there is also wedge boundaries in the case of OF). For the sake of uniformity, a velocity inlet of 10 m/s is adopted based on the input condition of 180 SLM. The Outlet condition is a pressure outlet, which is set as an atmosphere. As the source of ionization reactions, the Cathode should be assigned a relatively high boundary temperature

Table 2. Boundary conditions adopted for numerical simulation of magnetic fluid generation

Boundary part	**U** (m/s)	p (Pa)	T (K)	ϕ (V)	**A** (Tm)
Inlet	10	-	300	$\nabla\phi = 0$	$\nabla\mathbf{A} = 0$
Outlet	$\nabla\mathbf{U} = 0$	1×10^5	300	$\nabla\phi = 0$	0
Cathode	0	$\nabla p = 0$	3500	$\nabla\phi = -\mathbf{J}_{cath}/\sigma$	$\nabla\mathbf{A} = 0$
Anode	0	$\nabla p = 0$	$\kappa\nabla T = h_w(T - T_w)$	0	$\nabla\mathbf{A} = 0$
Wall	0	$\nabla p = 0$	$\kappa\nabla T = h_w(T - T_w)$	$\nabla\phi = 0$	$\nabla\mathbf{A} = 0$

of 3500K, yet it must remain below the melting point of tungsten, its material. Moreover, the Anode and Wall are no-slip wall and their boundary conditions are defined as a water-cooling condition:

$$-\kappa\nabla T = h_w(T_w - T) \tag{12}$$

where the value of heat transfer coefficient h_w and the reference surface temperature of the electrode T_w are set to 1.0×10^5 Wm–2K–1 and 500 K, respectively.

In particular, the setting of the electric potential boundary conditions of the Cathode and Anode determines the dynamic characteristics of the magnetic fluid. In this study, the flat tip conical shaped Cathode electric potential gradient is set to $-\mathbf{J}_{cath}/\sigma$, and the distribution of current density on its surface is in the form of an exponential profile of the current density $\mathbf{J}_{cath}$ as the following Eq. (13) [22, 23]. For Anode boundary condition, the electric potential ϕ is set as zero at the Anode surface.

$$\mathbf{J}_{cath} = J_{cath0}(\exp(-(\frac{r}{R_c})^{n_c})) \tag{13}$$

where r represents the radial position in the mesh, J_{cath0} is 2.5×10^8 Am–2, n_c is 4, and R_c is set to 0.4043 mm, then through the calculation using the following integral formula, it is clearly established that the input current to the generator is 114 A.

$$\mathbf{I} = \int_S \mathbf{J}_{cath}\mathrm{d}S \tag{14}$$

Finally, the magnetic vector potential is assumed to be zero at the Outlet, and a zero gradient boundary is applied at all other boundaries, while which inside the generator is governed by Eq. (5)

3.3. Calculation process

According to the governing equations in Section 2.2, the iterative solution process of the OF-based magnetic fluid solver can be summarized as follows:

I. Initialize all field values.
II. Enter the SIMPLE loop to update all physical properties according to the temperature field and start a new time-step iteration.
III. Solve the Poisson equation for the electric potential Eq. (4) to obtain the electric potential field.
IV. Solve the Ampere's law Eq. (5) to obtain the magnetic vector potential.

V. Solve the momentum conservation equation to obtain the pressure and velocity fields.

VI. Solve the energy conservation equation to obtain the temperature field.

VII. If the final time is not reached, return to step II.

The mass conservation Eq. (1), devoid of a time-dependent term and explicit variables, is not directly solved by the steady-state solver but instead serves primarily as a constraint [24, 25].

To solve the pressure-velocity coupling nonlinear equations, the SIMPLE algorithm is adopted by the solver. The superscript n represents the current iteration step (known), $*$ represents the prediction step (unknown); the subscript *P* represents the current grid unit, *N* represents the adjacent grid unit, f represents the value on the grid unit surface; V_P represents volume of the current grid unit; **S** represents the grid unit surface vector, and its iterative steps are as follows:

I. Initialize the SIMPLE calculation process a velocity field $\mathbf{U}^n$ and a pressure field p^n.

II. The predicted velocity $\mathbf{U}_P^*$ is obtained by solving the discrete momentum equation, which is called momentum predictor.

$$a_P^n \mathbf{U}_P^* + \sum a_N^n \mathbf{U}_N^* = -\frac{1}{V_P}\sum p_f^n \mathbf{S}_f \tag{15}$$

III. Introduce the assumption of omitting the influence of critical points and solve the pressure Poisson equation to obtain the corrected pressure p^*.

$$\nabla \cdot (\rho \frac{1}{a_P^n}(-\sum a_N^n \mathbf{U}_N^*)) = \nabla \cdot (\rho \frac{1}{a_P^n}\nabla p^*) \tag{16}$$

IV. Update the predicted velocity $\mathbf{U}_P^{**}$, which approximately satisfies the momentum equation.

$$\mathbf{U}_P^{**} = \frac{1}{a_P^n}(-\sum a_N^n \mathbf{U}_n^*) - \frac{1}{a_P^n}\frac{1}{V_P}\sum p_f^* \mathbf{S}_f \tag{17}$$

At this point, the original fields $\mathbf{U}^n$ and p^n are updated to $\mathbf{U}_P^{**}$ and p^* which means one iteration is completed and then repeat to convergence.

Before performing numerical simulation iterations, it is necessary to specifically incorporate and compile the thermophysical properties of argon magnetic fluid to the OpenFOAM library under thermophysicalModels. This involves implementing the properties-temperature linear interpolation method described in Section 2.3. The model uses hTableThermo to numerically characterize specific heat at constant pressure c_p, tableTransport to characterize molecular viscosity μ and thermal conductivity κ, and tableRho to characterize density ρ.

For the discrete methods of differential vector operators in the iterative process, the gradient is Gauss linear; the divergence is bounded Gauss limitedLinear 0.2; the Laplacian operator is Gauss linear orthogonal. For the solution of the linear equation system, the symmetric matrix GAMG with the DICGaussSeidel smoother is used to solve the pressure. The asymmetric matrix Stabilised preconditioned bi-conjugate gradient, PBiCGStab with the DILU or DIC predictor is used to solve other physical variables. In addition, as a steady-state solver, it is also necessary to apply matrix relaxation to each physical quantity to enhance stability.

The core of the magnetic fluid solver, based on the secondary development of Fluent, involves adding governing equations for the electromagnetic fields through User-Defined Scalar (UDS), incorporating source terms into the native N-S Equations and enthalpy conservation equation through User-Defined Function (UDF), and adding derived fields through C_UDMI, which also interpolates thermophysical properties based on properties-temperature tables and defines a flux boundary condition. The Fluent solver also uses the SIMPLE algorithm to solve the equations. Since the

addition of governing equations and source terms may easily lead to divergence in iterative calculations, it is essential to set a reasonable convergence residual and ensure that as small as possible pressure, momentum and energy relaxation factors are used.

4. Results Comparison and Analysis

Iterative calculations of the aforementioned magnetohydrodynamic model are performed using the OF solver and Fluent software, which yield the following physical field distributions.

4.1. Temperature distribution

The temperature distribution of the jet is of primary importance when preparing ceramic coatings using magnetic fluid. Ceramic powder materials with high melting points must melt quickly without significant vaporization. Therefore, it is crucial to maintain the magnetic fluid within an appropriate temperature range. The temperature distribution obtained from this numerical simulation is shown in Fig. 2, with details along the Axis presented in Fig. 4.

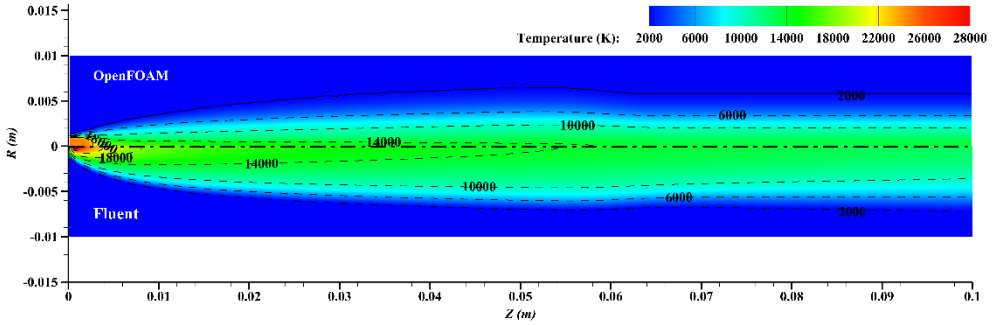

Figure 2. The distribution of the temperature of magnetic fluid

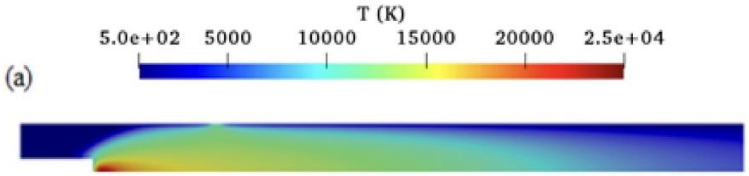

Figure 3. Temperature inside the generator from reference

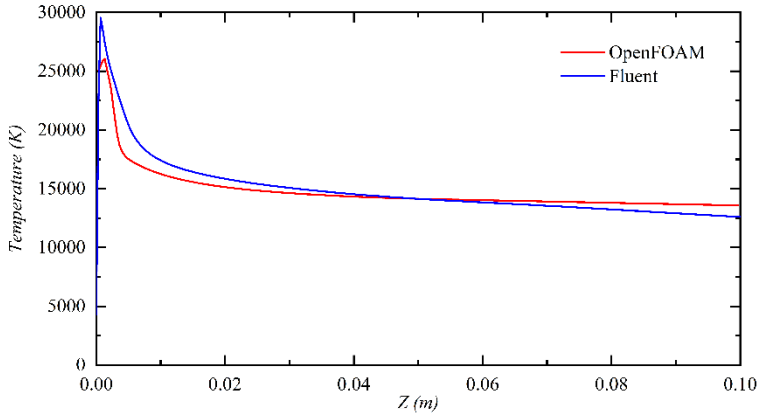

Figure 4. The distribution of the temperature along the Axis

It is revealed from Fig. 2 and Fig. 4 that the temperature distribution results of the OF solver and the Fluent are basically consistent with each other and with the findings of Perambadur [19] as shown in Fig. 3. The maximum temperature of the magnetic fluid is concentrated in the area near the axial Cathode. OF calculates the maximum cathode temperature of 27000 K, and Fluent calculates the cathode maximum temperature of 29000 K, which represents the upper temperature limit for thermophysical properties interpolation. With the Axis as the center, the temperature gradually decreases outwards. High-temperature regions are widely distributed along the axis, with the main body temperature above 6000 K. The temperature distribution in magnetic fluid is influenced by several factors, including cathode spots, current density, thermal conduction and convection, radiation and geometric symmetry. At the Cathode, arcs form small, high-temperature spots where the current is concentrated, leading to exceptionally high local temperature. During the arc discharge process, significant Joule heating and electron enthalpy are released, resulting in extremely high temperature, especially in areas with high current density. Heat from these high-temperature regions is conducted toward the surrounding water-cooling walls, while radiation losses further contribute to the gradual decrease in temperature outward from the center. Additionally, thermal convection driven by magnetohydrodynamic flow leads to a broader distribution of the high-temperature region along the axial direction.

The overall flow state is smooth and uniform. Both isotherms do not continue to expand in the area near the Anode, as the Anode exerts a compressive effect on the temperature field. In fact, several factors contribute to the convergence of the temperature field in the anode region, including arc constriction effects, the high thermal conductivity of anode material, fluid dynamic effects, concentrated current density, and material ablation and vaporization. However, based on the boundary conditions and the current density results, this convergence effect can primarily be attributed to the stronger electromagnetic field intensity, which causes arc constriction, leading to the accumulation of magnetic fluid in a smaller area near the anode.

4.2. Velocity distribution

The velocity of the molten metal droplets is a crucial factor in achieving high-quality surface coatings. Studies [26, 27] have demonstrated that high-speed molten droplets significantly enhance the adhesion, compactness, thermal barrier properties, wear resistance, and earthquake resistance of the coatings. Consequently, increasing the speed of the magnetic fluid is a major focus of research in this technology. Fig. 5 illustrates the velocity field distribution as studied through this numerical simulation, while Fig. 6 provides detailed information on the velocity along the Axis.

Fig. 5 and Fig. 6 illustrate that the velocity distribution results from both the OF solver and Fluent are generally consistent. The highest velocity in the domain occurs near the Cathode, with the OF solver reporting a maximum velocity of 260 m/s and Fluent reporting 290 m/s. Velocity decreases outward from the axis, maintaining a speed above 50 m/s throughout the main body of the flow. Fluent results clearly demonstrate an increase in magnetic fluid velocity in the anode region, and the axial velocity curve from the OF solver similarly shows a peak in the anode area.

In the cathode region, the interaction between the intense magnetic field and high current density generates a Lorentz force that acts perpendicular to both the current and magnetic field directions. This force accelerates the magnetic fluid along the Axis, resulting in maximum velocity near the cathode. Additionally, the high current density near the cathode causes localized high

temperatures, leading to significant thermal expansion, which further increases the flow velocity. In the anode region, the convergence of the electromagnetic field provides additional acceleration to the magnetic fluid. The compression of the temperature field facilitates further kinetic energy conversion, thereby increasing the velocity in this area. Throughout the flow process, the magnetic fluid efficiently converts electrical energy into kinetic energy, with energy losses through thermal conduction and radiation varying across different regions, thus influencing the overall velocity distribution.

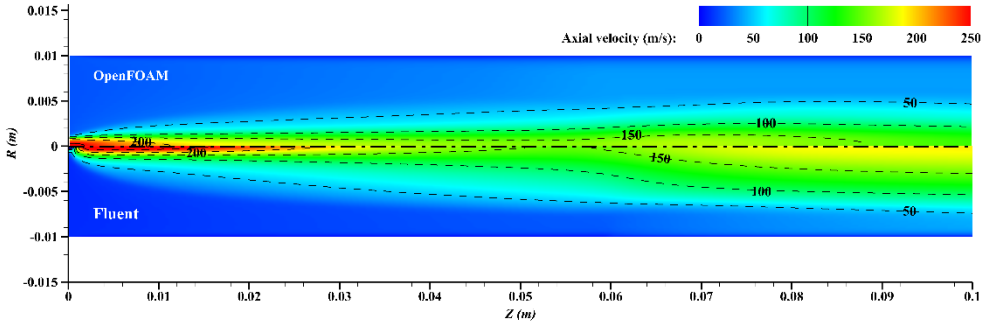

Figure 5. The distribution of the velocity of magnetic fluid

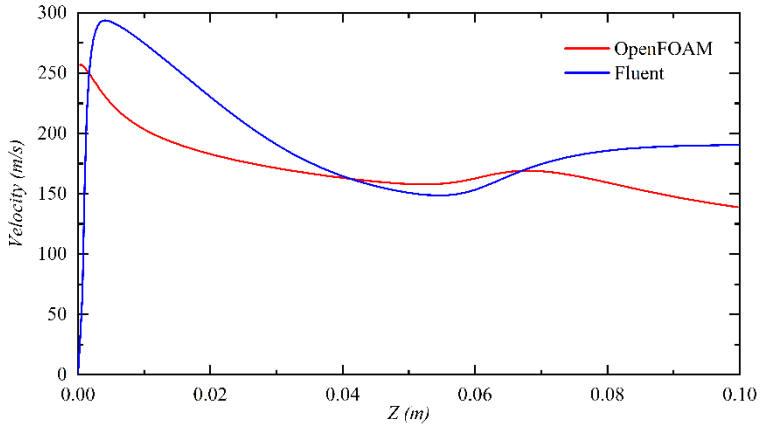

Figure 6. The distribution of the velocity along the Axis

4.3. Current density distribution

The electromagnetic field determines the dynamic characteristics of the magnetic fluid. On one hand, the Lorentz force directly influences the velocity field, while on the other, Joule heating and electron enthalpy from the ionization process directly impact the temperature field. The input to the electromagnetic field in this study is limited to the Cathode current density. Consequently, analyzing the current density distribution within the flow domain is essential for advancing investigation of magnetohydrodynamics. Fig. 7 shows the distribution of magnetic fluid current density, while Fig. 8 provides detailed information along the Axis.

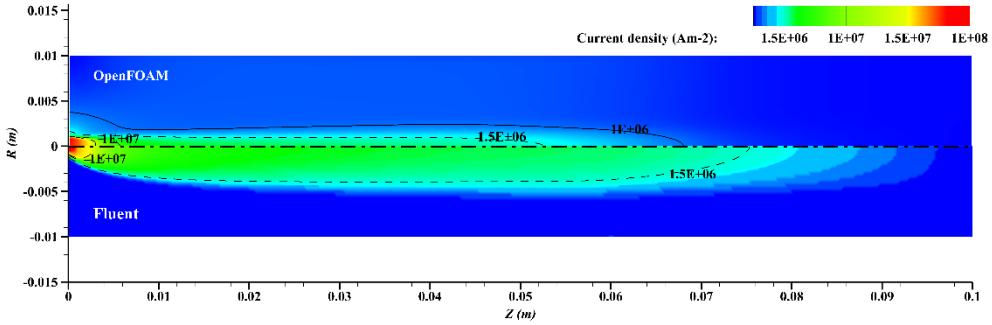

Figure 7. The distribution of the current density of magnetic fluid

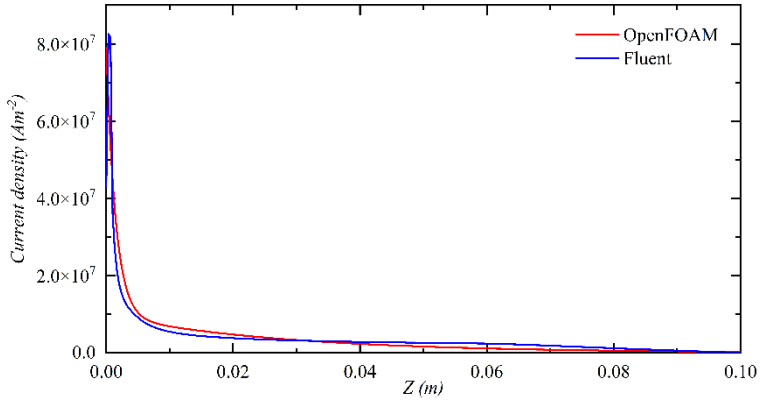

Figure 8. The distribution of the current density along the Axis

It is obvious that the current density is most concentrated in the region near the Cathode, exponentially decreasing along the axial direction until it diminishes near the anode, which also objectively confirms the validity and scientific accuracy of the velocity and temperature field distributions. Overall, the magnitude and radial-axial distribution of the current density computed using OF solver are less pronounced than those obtained with Fluent software. While the development of the OpenFOAM solver is consistent with Fluent in terms of implementation approach, replicating the precise details is challenging. As a result, further optimization tailored to specific conditions is necessary for simulating magnetic fluid phenomena using OpenFOAM.

5. Conclusions

Numerical simulations of a two-dimensional rotationally symmetric model of magnetic fluid are conducted using the originally developed OpenFOAM solver and the custom-developed Fluent. The study yields the following conclusions:

I. The numerical simulation results for magnetic fluid generation obtained with the OpenFOAM solver developed in this study are generally consistent with those from Fluent with secondary development.

II. The highest temperature of the magnetic fluid is observed near the Cathode, with the main body temperature exceeding 6000 K, and the Anode exerts a compressive effect on the temperature field.

III. The highest velocity of the magnetic fluid occurs near the Cathode, with the velocity further increasing in the axial direction near the Anode.

IV. The current density is concentrated near the Cathode, exponentially decreasing along the axial direction, and diminishes in the area near the Anode.

Based on magnetohydrodynamics theory, this study utilizes the development of an OpenFOAM solver and the secondary development of Fluent to provide foundational numerical simulation methods for the design and optimization of magnetic fluid industrial applications. However, further tuning and optimization are required for the OpenFOAM solver's effectiveness and detailed results. Additionally, more in-depth research is necessary in areas such as arc root attachment and three-dimensional compressible transient magnetohydrodynamic simulations.

Nomenclature

$\mathbf{A}$	magnetic vector potential, [Tm]
a	iteration coefficients matrix
$\mathbf{B}$	magnetic flux density, [T]
c_p	specific heat capacity at constant pressure, [Jkg–1K–1]
$\mathbf{E}$	electric field, [Vm–1]
e	electron charge, $1.602176634 \times 10^{-19}$ [C]
f	subscript, value on the grid unit surface
h	specific enthalpy, [Jkg–1]
h_w	coefficient of convective heat transfer, [Wm–2K–1]
$\mathbf{I}$	input current, [A]
$\mathbf{J}$	current density, [Am–2]
$\mathbf{J}_{cath}$	cathode current density, [Am–2]
J_{cath0}	coefficient of cathode current density, [Am–2]
k_B	Boltzmann constant, 1.380649×10^{-23} [JK–1]
N	subscript, adjacent grid unit
n	superscript, current iteration step
P	subscript, current grid unit
p	fluid pressure, [Pa]
r	cathode radius, [m]
$\mathbf{S}$	grid unit surface vector
T	fluid temperature, [K]
T_w	reference surface temperature, [K]
$\mathbf{U}$	fluid velocity, [m/s]
U_r	magnetic fluid thermal radiation loss, [Wm–3]
V_P	volume of current grid unit
ρ	fluid density, [kgm–3]
μ	molecular viscosity, [Pas]
κ	thermal conductivity, [Wm–1K–1]
σ	electric conductivity, [Sm–1]
ϕ	electric potential, [V]
μ_0	vacuum permeability, $1.25663706212 \times 10^{-6}$ [NA–2]

$*$ superscript, prediction step

References

[1] Ikpe, A. E., *et al.*, Material selection for high pressure (HP) turbine blade of conventional turbojet engines, *American journal of mechanical and industrial engineering, 1* (2016), 1, pp. 1-9

[2] Lima, R.S., *et al.*, Microstructural Characterization and Room-Temperature Erosion Behavior of As-Deposited SPS, EB-PVD and APS YSZ-Based TBCs, *Journal of Thermal Spray Technology, 28* (2019), pp. 223-232 https://doi.org/10.1007/s11666-018-0763-6

[3] Benjamin, B., *et al.*, Thermal insulation properties of YSZ coatings: Suspension Plasma Spraying (SPS) versus Electron Beam Physical Vapor Deposition (EB-PVD) and Atmospheric Plasma Spraying (APS), *Surface and Coatings Technology, 318* (2017), pp. 122-128 https://doi.org/10.1016/j.surfcoat.2016.06.010.

[4] Padture, N., *et al.*, Thermal barrier coatings for gas-turbine engine applications, *Science, 296* (2002), 5566, pp. 280-284 https://doi.org/10.1126/science.1068609

[5] Alagheband, A., Brown, C., Plasma Atomization goes commercial, *Metal Powder Report, 53* (1998), 11, pp. 26-28 https://doi.org/10.1016/S0026-0657(99)80007-1.

[6] Baskoro A.S., *et al.* Review on plasma atomizer technology for metal powder, *MATEC Web of Conferences 269*, (2019), 05004 https://doi.org/10.1051/matecconf/201926905004

[7] Lieberman M. A., Lichtenberg A. J., *Principles of plasma discharges and materials processing*, John Wiley & Sons Inc., Hoboken, New Jersey, Canada, 2005

[8] Chen F.F., *Introduction to plasma physics and controlled fusion*, Springer International Publishing, Cham, Switzerland, 2016

[9] Chazelas, C., *et al.*, Main Issues for a Fully Predictive Plasma Spray Torch Model and Numerical Considerations, *Plasma Chem Plasma Process, 37* (2017), pp. 627–651 https://doi.org/10.1007/s11090-017-9808-8

[10] Li HP., Chen X., Three-dimensional modelling of the flow and heat transfer in a laminar non-transferred arc plasma torch, *Chinese Physics, 11* (2002), 1, pp. 44-49 https://doi.org/10.1088/1009-1963/11/1/310

[11] Li, HP., Pfender, E., Three Dimensional Modeling of the Plasma Spray Process, *Journal of Thermal Spray Technology, 16* (2007), pp. 245-260 https://doi.org/10.1007/s11666-007-9023-x

[12] Hsu, K.C., A self-consistent model for the high intensity free-burning argon arc, Ph. D. thesis, University of Minnesota, Minneapolis, Minnesota, US, 1982.

[13] Chen, X. *Thermal plasma heat transfer and flow*, China Science Publishing & Media Ltd, Beijing, China, 2009 (in Chinese)

[14] Yin, Z., *et al.* Experimental and Numerical Analysis of a Reverse-polarity Plasma Torch for Plasma Atomization, *Plasma Chemistry and Plasma Process, 41* (2021) pp. 1471-1495 https://doi.org/10.1007/s11090-021-10181-8

[15] Sun, JH., *et al.* Two-Temperature Chemical Non-equilibrium Modeling of Argon DC Arc Plasma Torch, *Plasma Chemistry and Plasma Process 40* (2020) pp. 1383-1400 https://doi.org/10.1007/s11090-020-10108-9

[16] Sass-Tisovskaya M. Plasma arc welding simulation with OpenFOAM, Licentiate of Engineering, Chalmers University of Technology, Gothenburg, Sweden, 2009

[17] Godinaud N., *et al*. Development of a new OpenFOAM solver for plasma cutting modeling, *Computers & Fluids, 241* (2022), 105479 https://doi.org/10.1016/j.compfluid.2022.105479.

[18] Huang, R., et al. Simulation of Arc Root Fluctuation in a DC Non-Transferred Plasma Torch with Three Dimensional Modeling, Journal of Thermal Spray Technology, 21 (2012), 636–643 https://doi.org/10.1007/s11666-011-9710-5.

[19] Perambadur J., *et al.*, The investigation of arc fluctuations in thermal plasma torch using 3D modeling approach, *International Journal of Heat and Mass Transfer, 165* (2021), 120666 https://doi.org/10.1016/j.ijheatmasstransfer.2020.120666.

[20] Boulos, M.I., *et al. Handbook of Thermal Plasmas*, Springer International Publishing, Cham, Switzerland, 2023

[21] Choquet, I., ThermophysicalModels library in OpenFOAM-2.3.x How to implement a new thermophysical model, https://www.tfd.chalmers.se/~hani/kurser/OS_CFD_2014/isabelleChoquet/thermophysicalModels-OF-2.3-updated_HN141009.pdf

[22] Trelles, J.P., *et al.* Multiscale Finite Element Modeling of Arc Dynamics in a DC Plasma Torch, *Plasma Chem Plasma Process, 26* (2006), pp. 557-575 https://doi.org/10.1007/s11090-006-9023-5

[23] Alaya, M., *et al.* Arc-Cathode Coupling in the Modeling of a Conventional DC Plasma Spray Torch, *Journal of Thermal Spray Technology, 24* (2015), pp. 3-10 https://doi.org/10.1007/s11666-014-0162-6

[24] Jasak, H., OpenFOAM: Open source CFD in research and industry, *International Journal of Naval Architecture and Ocean Engineering, 1* (2009), 2, pp. 89-94 https://doi.org/10.2478/IJNAOE-2013-0011.

[25] Jasak, H. Error analysis and estimation for the finite volume method with applications to fluid flows, Ph. D. thesis, Imperial College, London, UK, 1996.

[26] Bai Y., *et al.*, High performance nanostructured ZrO2 based thermal barrier coatings deposited by high efficiency supersonic plasma spraying, *Applied Surface Science, 257* (2011) 16, pp. 7210-7216 https://doi.org/10.1016/j.apsusc.2011.03.092.

[27] Xi H., *et al.* Microstructure and mechanical properties of Mo coating deposited by supersonic plasma spraying, *International Journal of Refractory Metals and Hard Materials, 86* (2020), 105095 https://doi.org/10.1016/j.ijrmhm.2019.105095.

Submitted: 02.05.2024.
Revised: 07.08.2024.
Accepted: 12.08.2024.